Simulation of Ischemic Substrate Conditions Using a Model of the Human Atria

H. KRÄTSCHMER, B. HENSEL
Department of Biomedical Engineering, Friedrich-Alexander University Erlangen-Nuremberg, Erlangen, Germany

Summary

Despite a multitude of studies, the origin of atrial tachycardias is not yet completely understood. Above all, the causal connection between pathophysiologic tissue properties and the reentry kind has not yet been illuminated to date. The growing computing capacity of modern computer systems increasingly allows the modeling of complex electrophysiologic and biologic systems. This study focuses on modeling a tissue segment of the human atria as a basis for simulating pathophysiologic tissue properties. The influence of ischemia-induced changes on the formation of reentry circuits is at the center of the second part of this work. Ischemia-induced variations of the extracellular sodium concentrations and the permeability of the sodium channels were simulated. The spread of excitation as well as changes in the signal morphology were analyzed and evaluated in regard to the formation of a reentry. Reducing the extracellular sodium concentration as well as decreasing the sodium channels causes substrate changes that favor the formation of reentries. Additional decoupling of the atrial cells leads to a slower spread of excitation and thus favors the generation of reentries. An example is used to demonstrate the influence of ischemic substrate properties on the formation of reentries.

Key Words

Computer model, human atria, atrial tachycardia, ischemia, sodium channels

Introduction

Investigating the generation mechanisms of atrial tachycardias has been at the center of cardiovascular research for years. Therefore, it is of particular interest to deepen the understanding regarding the generation mechanism of atrial tachycardias. A clear causal connection between electrophysiologic conditions and the generation of reentries is of primary interest in this regard. Based on such knowledge, it would be possible to classify the atrial fibrillation of the patient, allowing the use of therapeutic measures with greater efficiency. Necessary experimental studies on the patient cannot be realized due to practical, ethical, and hygienic reasons. Thanks to the extensive computing power of modern computer systems, modeling is gaining more and more importance.

This study introduces a tissue model of the human atria that allows for an examination of the generation mechanisms of pathophysiologic excitation processes (reentries). Development of the model has to take into account modeling not only the cellular processes, but also cell coupling for the different myocardial regions. The complexity of the geometric model concerning the cell number determines the computing effort that is required. To keep it at an acceptable level, a compromise has to be found regarding the cell number and the cell size of the model. Therefore, every modeled cell represents an aggregation of real cells. The influence of the cell size on the spread of excitation is a central problem in modeling. Based on the generated model, the influence of a pathophysiologic excitability on the

signal morphology and the spread of excitation are studied while considering a physiologic and a pathophysiologic cell coupling.

Models

Model of Human Atrial Tissue

The simulation of atrial conduction sequences requires a model in which the properties of the human atrial myocardium are considered: A realistic cell model is used for describing the atrial action potential [1]. The spread of excitation needs to be realized by a cell coupling according to the diffusive processes via the gap junctions [2,3]. Finally, the computing effort should be acceptable. In the following, the model is explained in detail.

Atrial Cell Model

The electrophysiologic properties of a human atrial cell are described by the model of Nygren et al. [1]. In this model, the detailed description of the ion-exchange between the extra- and intracellular space is based on the Hodgkin – Huxley equation [4,5]. Based on that equation, six time-dependent ion currents (I_{Na}, I_{CaL}, I_t, I_{sus}, I_{Kr}, I_{Ks}), the voltage-dependent potassium current I_{K1} , the Na^+ – Ca^{2+} exchanger currents responsible for maintaining intracellular ion concentrations (I_{CaP}, I_{NaK}, I_{NaCa}), the Ca^{2+}- and Na^+- K^+ pump, and the Ca^{2+} and Na^+ background currents ($I_{B,Na}$, $I_{B,Ca}$) contribute to the action potentials. In Figure 1, the electrical equivalent circuit of the sarcolemma of the human atrial cell is represented. For the description of the ion

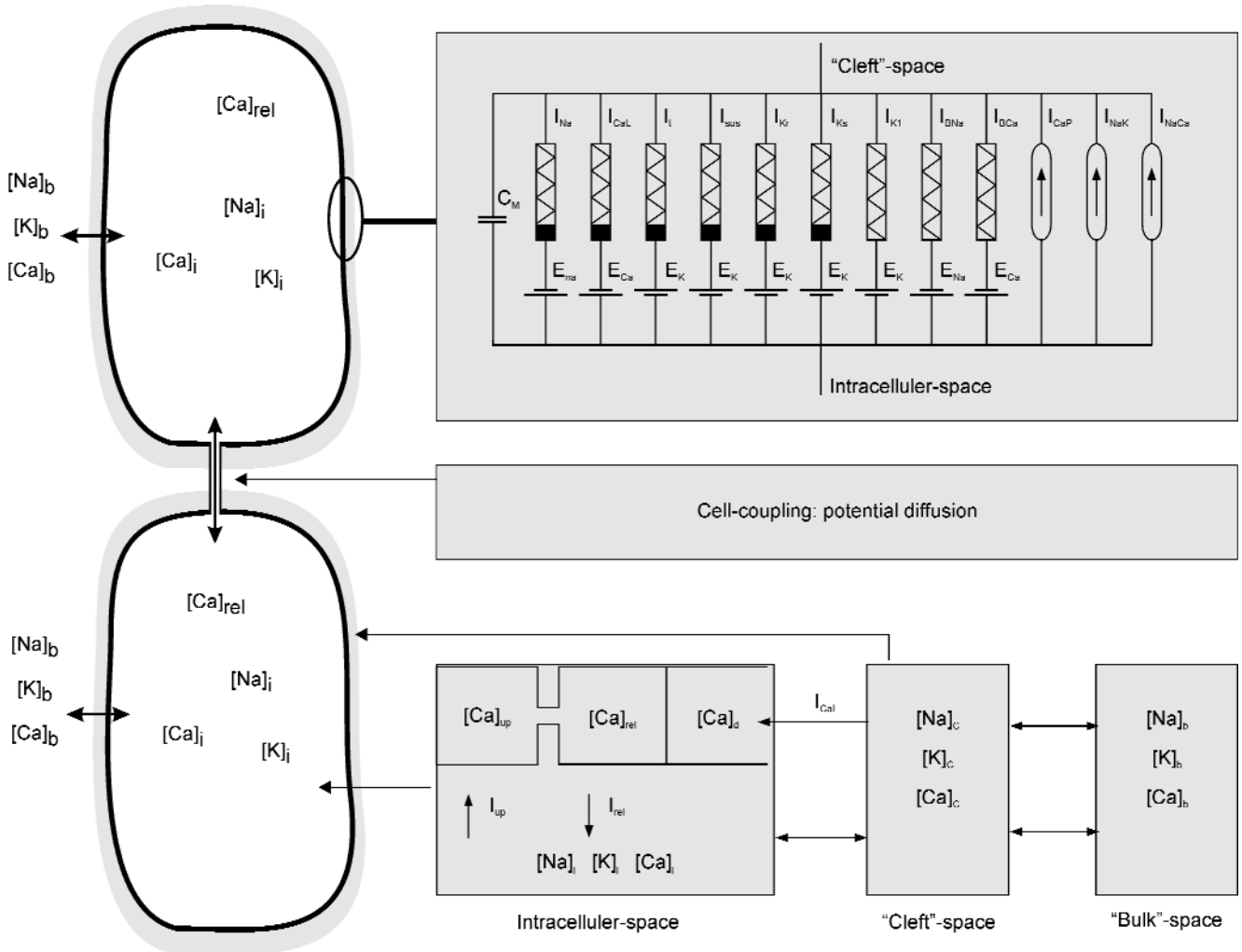

Figure 1. Schematic depiction of the model of coupled human atrial cells. The cell membrane is shown in an electrical equivalent circuit diagram, the intra- and extracellular space in a compartment model, and the cell coupling in a potential diffusion.

exchange, it is coupled with a fluid compartment model, including intracellular and extracellular spaces. The partition of the extracellular space into a bulk and a cleft space considers the constrained diffusion of ions from and to the cell membrane. Additionally, intracellular Ca^{2+} currents and ion concentrations in the sarcoplasmatic reticulum are taken into account. The time dependence of the resulting action potential arises from 29 partial differential equations. For detailed information, refer to the paper of Nygren et al. [1].

Spread of Excitation

The spread of excitation in the myocardium is based on cellular coupling via various types of gap junctions [2,3]. Thereby, ions diffuse from one cell to all neighboring cells as a result of a potential and ion concentration gradient. The mathematical description of such a diffusion problem is governed by a so-called reaction diffusion equation, which can be written for a continuous substrate as follows [5]:

$$\frac{dU}{dt} = \nabla(D\nabla U) + f$$

With this approach, the diffusion controlled by the diffusion constant D and the source with a potential rate (f) are considered. Although the cellular coupling in the atrial myocardium is anisotropic [6,7], investigations demonstrated that the excitation velocity in a healthy heart is independent of the direction of the excitation. Thus, in the presented model an isotropic diffusion is realized, which is independent of direction and position. Therefore, D is represented by a constant value. The description of the diffusion succeeds only by considering the properties of the geometric mesh. The regular mesh was modeled from triangles. To describe the diffusion, so-called Voronoi polygons were introduced, connecting each nodal point of the triangulated mesh with such a polygon [8,9]. The corner points of the Voronoi polygons are the intersections of the central vertical of the individual triangle sides of the Delaunay triangles. Prerequisite for the formation of such Voronoi polygons is the fact that these intersections lie inside the triangles. This condition is met exactly then if the triangles are so-called Delaunay triangles, i.e., all inside angles of a triangle are smaller than 90°. Figure 2 shows a section of a mesh consisting of Delaunay triangles and the corresponding Voronoi polygons (grey mesh). In the model, diffusion takes place from one nodal point to the next. Every involved Voronoi polygon constitutes an equipotential area, so that the diffusion occurs along a linear potential gradient. Aside from the distance L_{ij} between two neighboring Voronoi cells (nodal points), their size Λ_i influences the diffusion. Thus, different charge amounts of differently sized cells are accounted for. Finally, the potential amount diffusing to the neighboring cell j is determined by the length of shared edge λ_{ij} of two Voronoi polygons, thus taking into consideration the varying contact line between two cells. The model only considers an isotropic diffusion, which can be approximated by the approach

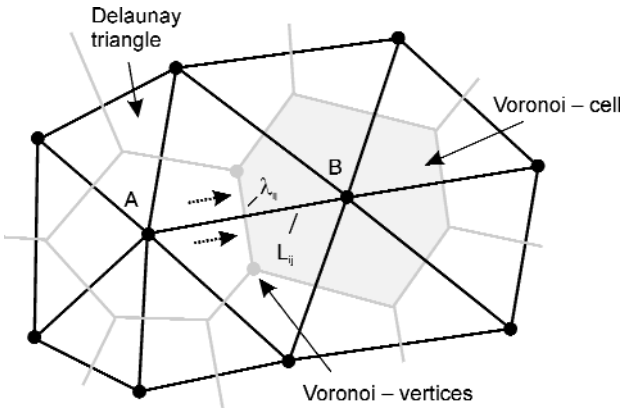

Figure 2. Section of a mesh consisting of Delaunay triangles with the corresponding Voronoi polygons. The diffusion from nodal point A to B is based on the potential gradient along L_{ij}. The actual current is determined by, among others, the size of the shared edge λ_{ij}.

$$\frac{dU_i}{dt} = -\sum_{j=1}^{N_i} D\frac{\lambda_{ij}}{\Lambda_i L_{ij}}\left(U_i - U_j\right)$$

(D = distance between two cells and their edge; U_i and U_j = potential of the cells i and j).

In the model, each nodal point of the triangulated mesh constitutes a Nygren cell. Linking takes place through the described reaction-diffusion equation. The strength of the cell coupling is adjusted through the diffusion constant. Therefore, a faster spread of excitation is realized by a higher diffusion constant.

Geometrical Mesh
A 4 x 5 cm^2 planar tissue model consisting solely of equidistant Delaunay triangles and describing a section of the atrial tissue was developed for simulation. The cell size was varied for differing simulations between 0.2 cm and 0.025 cm. Thus each modeled cell describes an entire cell aggregation of real cells to keep the computing effort as low as possible. Care has to be taken to make sure that the cell size does not influence the signal morphology of the action potential too much. For a cell size of 0.1 cm, the area is made up of 4,545 triangles with 3,269 nodal points (Voronoi cells). When cutting the distance in half, the number of nodal points quadruples.

Simulations

An excitation front is generated by stimulating a cell aggregation with an area of 0.5 x 0.3 cm^2 in the center of one of the two long side edges of the planar model. To this end, the potential is raised suddenly to 50 mV for a duration of 2 ms. The edges of the tissue model show no-flux conditions in regard to the potential diffusion and thus have a reflecting effect. For this reason, the model was designed sufficiently wide to avoid influencing the spread of excitation in the center. At the beginning of each simulation, the tissue model is in a state of rest with a potential of -74 mV.

Influence of Cell Dimensions on Signal Morphology
To analyze the influence of the potential diffusion on the signal morphology, the action potentials were recorded for tissue models consisting of Delaunay triangles with differing cell distances (cell size: 0.2 cm; 0.1 cm; 0.05 cm; 0.025 cm). To this end, a measuring electrode was defined at a distance of 2.5 cm from the electrode. The recorded signals were analyzed regarding the following parameters: the velocity of the excitation spread (VP), the maximum amplitude (AMP), the maximum upstroke velocity $(dV/dt)_{max}$, and the action potential duration (APD90) – the time interval between the point of the maximum upstroke and the point in time when the action potential has decreased to 90% – as well as the upstroke time Δt that describes the depolarization period between -60 mV and 0 mV. The simulations were carried out using physiologic cell characteristics and a physiologic cell coupling.

Influence of Cell Dimensions on Wave Front Morphology
To examine the wave front in relation to the cell size, the model described above was used. At a distance of 0.5 cm vertically to the electrode, a number of measuring points were positioned over a distance of 1 cm to allow capturing the course of the excitation front. The simulations were carried out under physiologic cell characteristics and a physiologic cell coupling. The cell size was varied between 0.025 cm and 0.2 cm (cell size: 0.2 cm; 0.1 cm; 0.05 cm; 0.025 cm).

Ischemic Substrate Properties
Ischemic tissue is primarily characterized by a reduced excitability [10-12] caused by a diminished sodium influx I_{Na}. This is the result of either a decreased permeability of the sodium channels or a low concentration gradient between the extracellular and intracellular sodium concentrations. To simulate ischemic substrate properties, the model with a cell size of 0.05 cm was used. First, the extracellular sodium concentration was varied in steps of 13 mmol/l from 78 mmol/l (60%) to 156 mmol/l (120%). Next, the permeability of the sodium channels was varied between 0.0016 nl/s (100%) and 0.00096 nl/s (60%). The cell couplings (D = 1, 2, 3) were varied for each of these settings. The provoked changes in the spread of excitation and the signal morphology were analyzed using the previously described parameters (VP, APD90, $(dV/dt)_{max}$) and the position of the vulnerable window. For each parameter variation, the wavelength Λ was determined from the product of VP and position of the vulnerable window as a measure for the formation of reentries.

Influence of Ischemic Substrate Properties on the Generation of Reentries
The influence on initiating a reentry can be tested by delivering an additional stimulus at the back of an excitation front. If the tissue is in its relative refractory period at this time, a new excitation front is formed that spreads in opposite direction to the initial one. Under the right conditions, this leads to a reentry [13-15]. This scenario was simulated with the tissue model (cell size = 0.05 cm). In the center of the total area, an area of equal size, a second stimulation electrode (SE2) was placed. At the time t = 0, the tissue was stimulated at an edge. At the time when the tissue at the location of SE2 is in the vulnerable window, a second stimulus is delivered there. The simulation was performed

under physiologic conditions (cell coupling: D = 3; $[Na^+]_C$ = 100%) as well as under pathophysiologic properties (D = 1, $[Na^+]_C$ = 80%).

Results

Influence of Cell Dimensions on Signal Morphology

At a cell size of 0.1 cm and 0.2 cm, a delay is seen at the beginning of the upstroke (Figure 3a). This behavior can be explained by the fact that the potential diffusion becomes slower with increasing cell size. In larger cells, less potential diffuses per time unit than in smaller cells, so that the membrane potential increases only slowly at first. After the threshold potential of approximately -35 mV has been reached, automatic depolarization takes place, and (dV/dt) increases. While an upstroke time of 1.4 ms and 1.5 ms, respectively, results for cell sizes of 0.025 cm and 0.05 cm, Δt is four times larger with 5.7 ms for a cell size of 0.2 cm. Thus, the upstroke is more sluggish in larger cells. The action potential duration shows a lengthening from 242 ms (cell size = 0.025 cm) to 261 ms (cell size = 0.2 cm) with increasing cell size. The voltage-dependent repolarization currents I_{sus}, I_{Kr}, and I_{Ks} of the atrial cell are started later due to the slower potential diffusion, delaying the repolarization. Both $(dV/dt)_{max}$ and the maximum amplitude do not show any conclusive dependencies from the cell size, even though $(dV/dt)_{max}$ shows a tendency to increase with the cell size. Therefore, the influence of the cell size on signal morphology decreases with the cell size. For cells under 0.1 cm, the influence is very small, suggesting the selection of a cell size between 0.05 cm and 0.1 cm for modeling an atrial tissue.

Influence of Cell Dimensions on Wave Front Morphology

The influence of the cell size on an excitation front is graphically depicted in Figure 3b. With increasing cell size, the width of the wave front increases, and thus the gradient decreases. The dependency on the cell size decreases with the cell size. Hardly any changes can be found for cells < 0.1 cm (width of wave front for a cell size of 0.025 cm and 0.05 cm: 0.15 cm and 0.16 cm). Clearly, wider excitation fronts with 0.22 cm and 0.37 cm, respectively, result in a cell distance of 0.1 cm and 0.2 cm. There are two reasons for this. First, the potential diffusion from one cell to another per time unit diminishes with increasing distance. Second, the increasing cell size has a self-limiting effect in a way, because the width of the wave front has to be at least the cell size width. For small cells, it follows that the width of the wave front does not decrease arbitrarily with the cell size but possesses a finite width and covers several cells. To simulate excitation processes, it is important for the excitation front to have a width that shows the lowest possible dependency on the cell size. Corresponding to the previous results, it is sufficient to select a cell size between 0.05 cm and 0.1 cm for modeling a piece of atrial tissue. Each of these cells will then describe a cell aggregation of real cells. A cell with a size of 0.05 cm describes an aggregation of about 430 real cells.

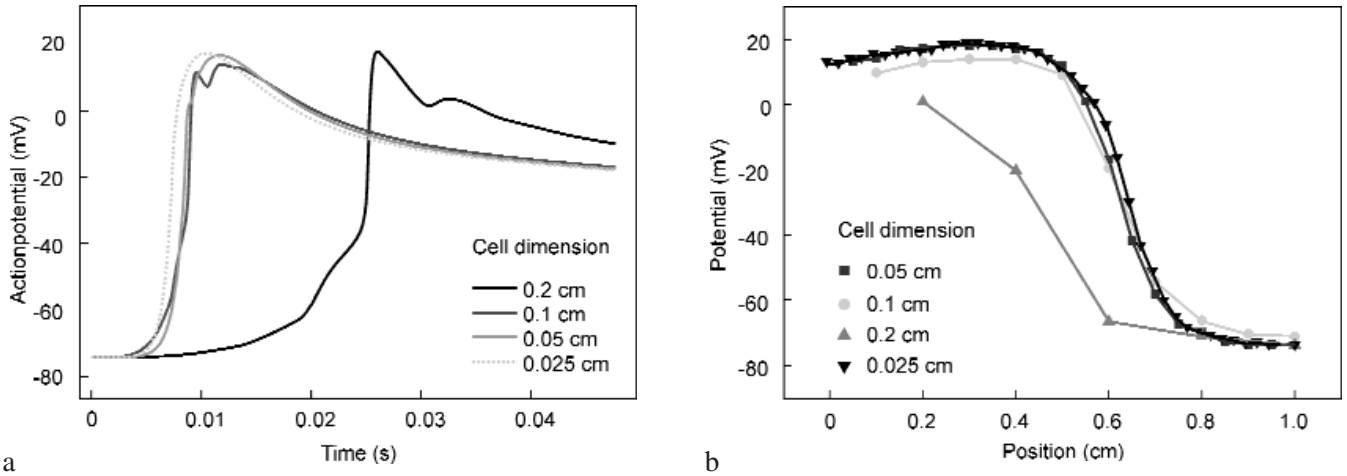

Figure 3. Panel a) Depolarization gradient of simulated action potentials for different cell sizes at D = 2. Panel b) Cross-sections of the wave front for different cell sizes.

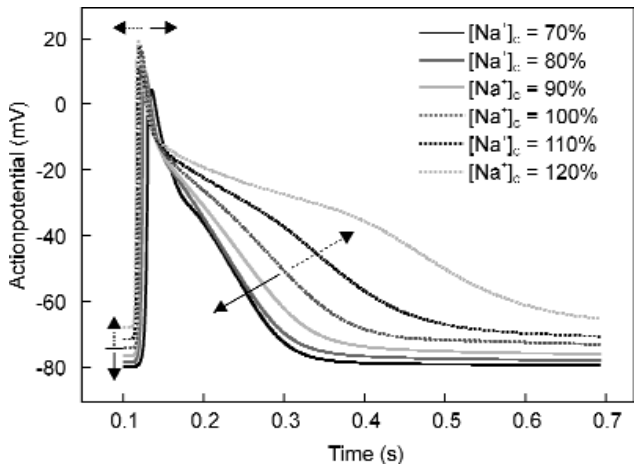

Figure 4. Simulated action potentials for different extracellular sodium concentrations at physiologic cell coupling. The arrows indicate the corresponding specific changes for an increase (dashed arrow) or decrease of $[Na^+]_C$.

Ischemic Substrate Properties/Variation of the Extracellular Sodium Concentration

Figure 4 shows the course of simulated action potentials for various sodium concentrations. The variation of $[Na^+]_C$ affects the signal morphology in three ways:

- It leads to a shift in the sodium-specific Nernst potential, which in turn affects the resting potential of the cell membrane. A reduction of $[Na^+]_C$ results in a lowering of the resting potential. Starting with -74.28 mV for a physiologic $[Na^+]_C$, a resting potential of -79.95 mV results in $[Na^+]_C$ = 91 mmol/l (70%). In case of an increase to 156 mmol/l (120%), the resting potential rises to a value of -67.98 mV an. This change leads to a different threshold response.
- The variation of $[Na^+]_C$ changes the concentration-driven ion influx and influences the behavior of all

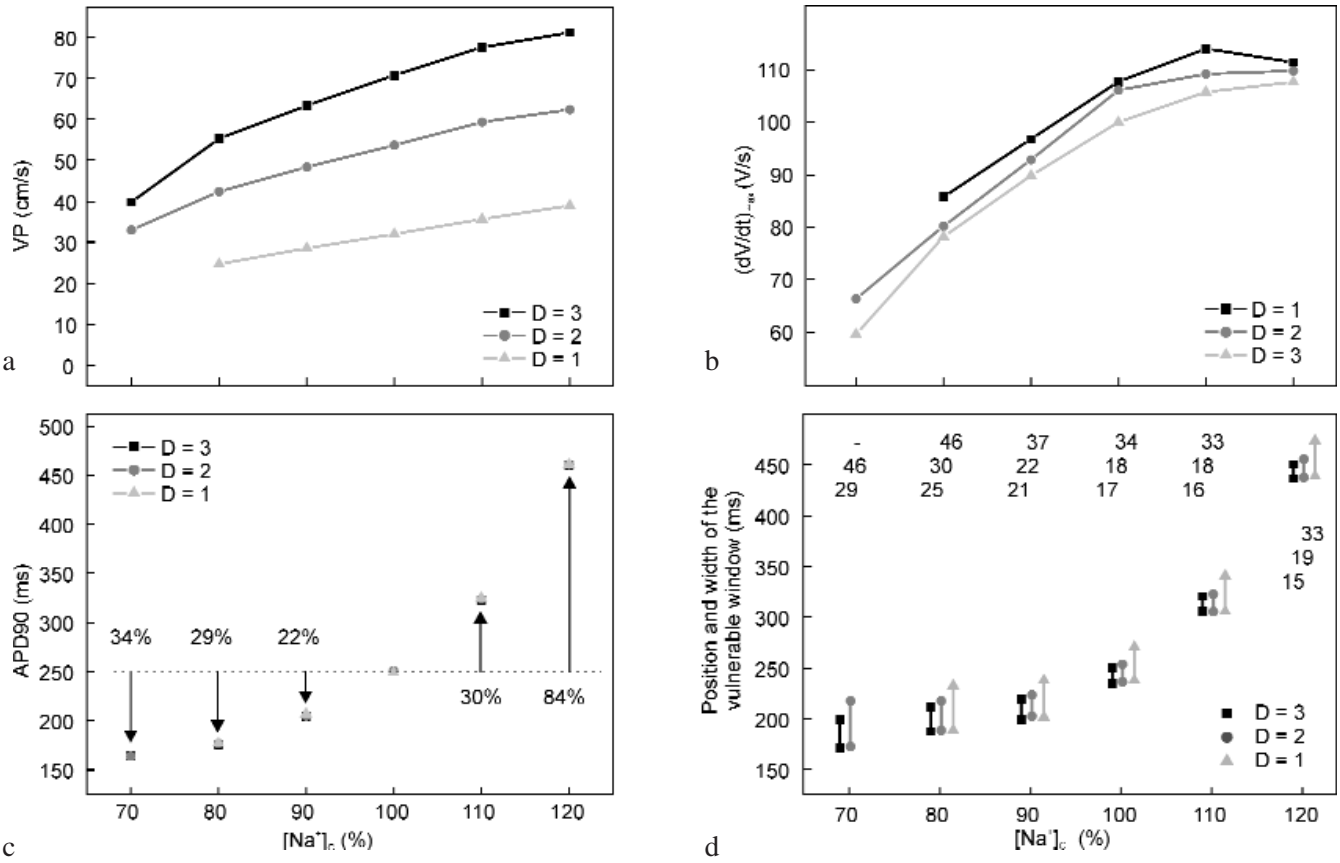

Figure 5. Simulation results for different $[Na^+]_C$ depending on the cell coupling: panel a) velocity of the excitation spread, panel b) maximum depolarization gradient, panel c) action potential duration, and panel d) position and width of the vulnerable window.

gate variables. With a higher $[Na^+]_C$, all this leads to a faster depolarization and thus better excitability. To compensate for the stronger depolarization, the repolarizing potassium currents I_t and I_{sus} are also larger and longer lasting at a higher $[Na^+]_C$.

- Due to the equilibrium of the longer-lasting currents I_{sus} and $I_{Ca\text{-}L}$, pronounced plateaus and, therefore, a longer action potential results in a higher $[Na^+]_C$.

The quantitative effects of varying $[Na^+]_C$ on the morphology of the action potential and the spread of excitation are shown in Figure 5 for different cell couplings. The maximum depolarization gradient (D = 3) increases with $[Na^+]_C$ from 59.6 V/s at 91 mmol/l (70%) to 105.8 V/S at 156 mmol/l (120%). A reduced $[Na^+]_C$ has a strongly inhibiting influence on the depolarization. With decreasing cell coupling, the depolarization gradient increases independent of $[Na^+]_C$. Thus, variation of $[Na^+]_C$ shows no significant influence on the cell coupling. Only at a $[Na^+]_C$ of 91 mmol/l (70%), no excitation could be generated for a low cell coupling (D < 2). Reducing the cleft-space sodium concentration ($[Na^+]_C$) to a value of 78 mmol/l (60%) leads to a conduction block independent of the cell coupling. The low $[Na^+]_C$ decreases the resting potential so much that the threshold is not reached because of the lower concentration gradient of $[Na^+]_C$.The decrease in excitability with decreasing $[Na^+]_C$ has a direct effect on VP (Figure 5a). With $[Na^+]_C$ > 130 mmol/l (100%), the VP increases from 70.8 cm/s to 81.2 cm/s for 156 mmol/l (120%; D = 3). When reducing to $[Na^+]_C$ = 91 mmol/l (70%), the VP drops to 39.8 cm/s. Less cell coupling leads to lower VPs. For D = 1 a conduction block results in $[Na^+]_C$ = 91 mmol/l (70%), making it impossible to state a VP in this case.

D (a.u.)	Wave lenght (cm) subject to $[Na^+]_C$					
	70%	80%	90%	100%	110%	120%
1	-	4.7	5.8	7.6	10.9	17.1
2	5.7	8.0	9.8	12.7	18.2	27.3
3	6.8	10.4	12.7	16.6	23.7	35.5

a

D (a.u.)	Wave lenght (cm) subject to PNa				
	60%	70%	80%	90%	100%
1	5.6	6.4	7.0	7.5	10.9
2	10.5	11.9	12.5	12.9	12.7
3	10.5	14.9	15.9	15.9	26.6

b

Table 1. Characteristic wave length depending on the cell coupling for a tissue with different $[Na^+]_C$ (panel a) and PNA (panel b). a.u. = arbitrary units; D = diffusion constant.

Figure 5c shows the APD90 in relation to $[Na^+]_C$ for various diffusion constants. The action potential lengthens by 84% to 460 ms when increasing $[Na^+]_C$ to 156 mmol/l (120%). A reduction of $[Na^+]_C$ to 91 mmol/l (70%) leads to a shortening by 34% to 165 ms. Simultaneously lessening the cell coupling results in no significant change of the action potential duration. This has consequences for the position and width of the vulnerable window (Figure 5d). The position (beginning) of the vulnerable window is related to the time of the corresponding maximum depolarization gradient. Consequently, the position shifts from 172 ms for $[Na^+]_C$ = 91 mmol/l (70%; D = 3) to 437 ms for 156 mmol/l (120%; D = 3). At the same time, the width decreases from 29 ms to 15 ms. With a low cell coupling, the position of the vulnerable window shifts only by 1 – 2 ms. However, the duration of the vulnerable window increases markedly.

Table 1a lists the resulting wavelengths for different $[Na^+]_C$. The lowest values result in low $[Na^+]_C$ and simultaneous decoupling. Thus, the formation of reentries becomes more probable with decreasing $[Na^+]_C$. The reduction in the velocity of the excitation spread as well as the shortening of the refractory period have the consequence that excitation fronts will again meet excitable tissue after circling a barrier. The formation of reentries becomes more likely with increasing ischemia.

Ischemic Substrate Properties/Restricted Permeability of the Sodium Channel

Reducing the PNa leads to a decreased depolarization ability and a delay in the repolarization ability, resulting in a conduction block at PNa = 0.00096 nl/s (Figure 6). In contrast to varying $[Na^+]_C$, the reduction of the PNa does not affect a shift of the resting potential. The lower I_{Na} leads to a slower depolarization, just as in the case of a lower $[Na^+]_C$. Furthermore, a lengthening of the action potential and the formation of a larger plateau can be observed with a lower PNa.

The quantitative simulation results regarding the maximum excitability are graphically depicted in Figure 7b. With decreasing PNa, the sodium influx decreases and thus the excitation velocity, starting from 100 V/s for PNa = 0.0016 nl/s (100%) to 41.4 V/s for

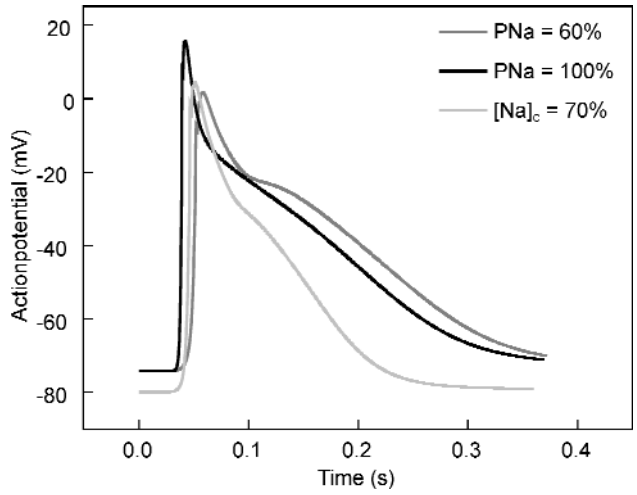

Figure 6. Simulated action potentials for a reduced and a physiologic PNa, as well as for a reduced $[Na^+]_C$.

PNa = 0.00096 nl/s (60%) at a cell coupling of $D = 3$. Decreasing cell coupling itself has an enhancing effect on $(dV/dt)_{max}$, increasing it to a value of 47.4 V/s for $D = 2$ and 50.6 V/s for $D = 1$ at a permeability of 60%. The direct comparison to the $(dV/dt)_{max}$ in case of the same percentage of reduction of $[Na^+]_C$ shows an amazing congruence. For example, the maximum excitability at $[Na^+]_C$ = 70% is 59.6 V/s, and at PNa = 70%, $(dV/dt)_{max}$ = 60.3 V/s. The maximum excitability therefore changes in case of a reduction of $[Na^+]_C$, starting at physiologic conditions, to the same degree than in case of a reduction of the PNa.

Resulting from the diminishing excitability of the cells, the spread of excitation increasingly slows down at a lower PNa. The VP drops from 70.8 cm/s at PNa = 0.0016 nl/s (100%) to 32.8 cm/s at PNa = 0.00096 nl/s (60%). At a permeability below 60%, a conduction block occurs, because the sodium

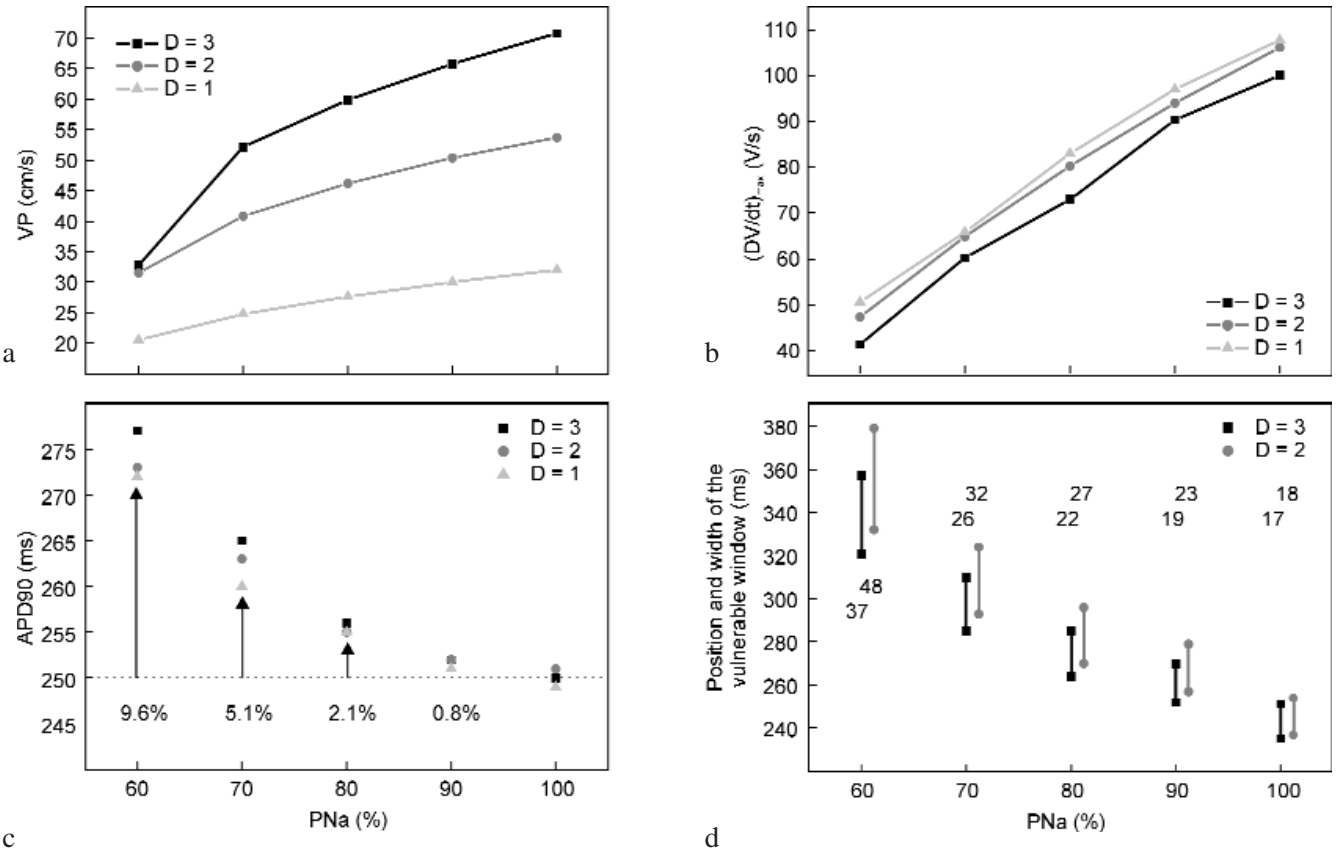

Figure 7. Simulation results for different PNa depending on the cell coupling: panel a) velocity of the excitation spread, panel b) maximum depolarization gradient, panel c) action potential duration, and panel d) position and width of the vulnerable window.

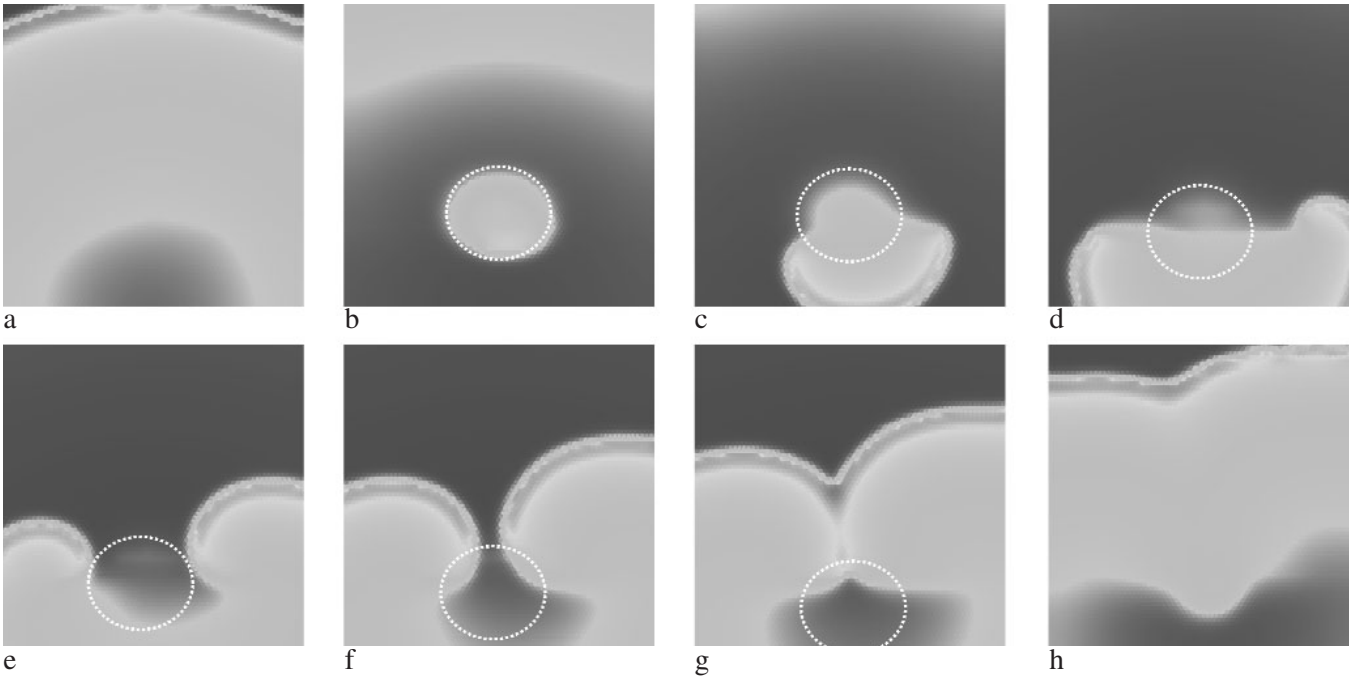

Figure 8. Generation mechanism of a reentry. The individual images show the excitation at intervals of 100 ms. After a continuing excitation front has spread with a velocity of ca. 53.7 cm/s (D = 2) from below to above (panel a), the tissue is re-excited by an atrial extrasystole (second stimulus) (panel b). Due to the unidirectional block, the excitation spreads in a half-moon shape around a functional barrier (dotted circle; panels c and d). The two wavefronts meet above the barrier and unite. Since the tissue below is still refractory, an excitation front only spreads in the upper direction.

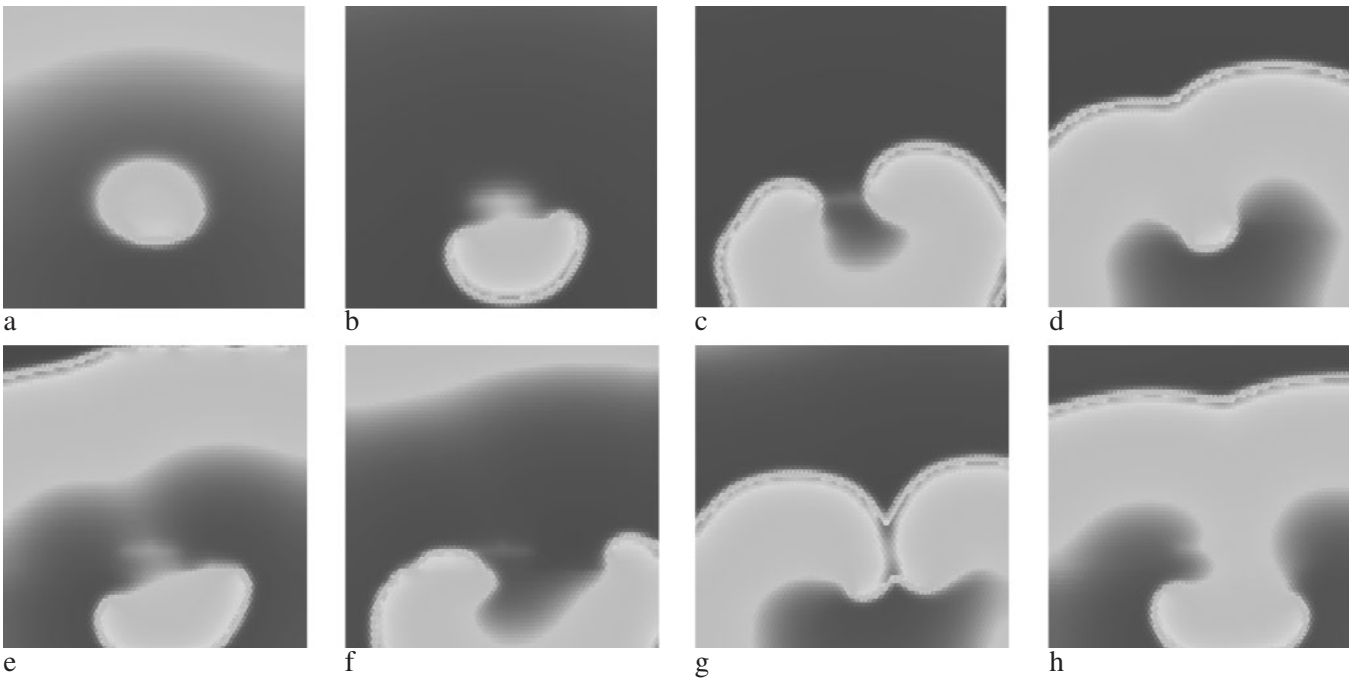

Figure 9. Simulation of a rotor formation under pathophysiologic tissue properties. The individual images show the excitation at intervals of 100 ms. The cell coupling was reduced to D = 1 and the extracellular sodium concentration to 80%, resulting in an excitation spread velocity of 25 cm/s. The second stimulus occurred 270 ms after the first excitation. Due to the pathophysiologic tissue properties, the tissue below the meeting point of the two excitation fronts is again in an excitable state (panel d), leading to reentry circuits.

influx is too low to reach the threshold potential. Thus the lowest VP is achieved with PNa = 0.00096 nl/s (60%). With decreasing cell coupling, the VP slows down accordingly, with a diminishing influence of the cell coupling. Thus, a VP of 32 cm/s results in D = 1 and PNa = 100%. For PNa = 0.00096 nl/s (60%), the VP is reduced to 20.5 cm/s.

A reduced PNa causes a lengthening of the corresponding action potentials, which can be explained by the increasingly longer activation of the Ca L-type and potassium channels. For PNa = 0.00096 nl/s (60%), the APD90 is lengthened by 9.6% to 274 ms (average for all D). The influence of the cell coupling slightly increases with decreasing permeability.

Figure 7d shows the position and width of the vulnerable windows in relation to the PNa. The width of the window increases with PNa decreasing from 0.0016 nl/s (100%) to 0.00096 nl/s (60%) from 17 ms to 37 ms for D = 3, and from 18 ms to 48 ms for D = 2. At the same time, the position of the vulnerable window shifts from 236 ms to 321 ms (D = 3) and 332 ms (D = 2), respectively.

The observed lengthening of the action potentials at reduced PNa leads, despite a lower velocity of the spread of excitation, to longer wavelengths compared to those at lower $[Na^+]_C$. Table 1b summarizes all wavelengths Λ(vw) in relation to the PNa for different D. Just reducing the permeability to 0.00096 nl/s (60%) leads to a wavelength of 10.5 cm at a physiologic cell coupling (D = 3). Additional partial decoupling of the cells (D = 1) reduces Λ(vw) to 5.6 cm. Compared to this, the shortest wavelength that results from a reduced $[Na^+]_C$ is 4.7 cm. Thus, the reduction of $[Na^+]_C$ supports the generation of reentries more than the lowering of the PNa. Only with a strong decoupling of the cells, the velocity of the excitation spread drops so low that reentries become probable at a reduced PNa.

Influence of Ischemic Substrate Properties on the Generation of Reentries

Physiologic substrate properties: Figure 8 graphically depicts the simulation result with a sequence of images. Starting at the SE2, the tissue was re-stimulated 280 ms after the first excitation front. At this time the tissue around the SE2 is in the relative refractory period, making it impossible to excite the area above (unidirectional block), and the new excitation only spreads into the opposite direction. The following pictures show how the excitation first spreads in a half-circle opposite to the first excitation wave and then on both sides around the area of the SE2. This area temporarily constitutes a functional barrier, until the tissue is repolarized and can again be excited. Subsequently, both bent excitation waves run towards the center. However, since the area below the meeting point of the two excitation fronts is still refractory, the excitation front is blocked below. Thus the reentry destroys itself already after only one circulation. Therefore, no reentry can be generated under physiologic conditions without sufficiently large barriers.

Pathophysiologic substrate properties: According to the results presented above, the simultaneous reduction of the extracellular sodium concentration and the cell coupling leads to a reduced velocity of the excitation spread and a shortening of the action potential. Thus the tissue below the meeting point of the two excitation fronts is not refractory, and an excitation can spread into this direction, too (Figure 9 d and e). In the following pictures, the described process is repeated, whereby it has to be noted that the centers of the rotors wander. The simultaneous reduction of the velocity of the excitation spread to 25 cm/s and the extracellular sodium concentration to 80% affect a shortening of the wavelength to 4.7 cm. Thus, pathophysiologic substrate properties result that enable the formation of stable rotors or reentries.

Conclusion

This study presented the modeling of a tissue segment of human atria. The electrophysiologic properties of atrial cells are described by the cell model according to Nygren et al. [1] and by a diffusive cell coupling. The model is limited by the cell size, which describes a cell aggregation of real cells. However, the simulations have shown that the signal morphology and the spread of excitation are only slightly influenced below a critical cell size of 0.1 cm. The simulation of ischemic substrate properties has shown that the reduction of the extracellular sodium concentration as well as of the Na-channel conductivity change the substrate properties in such a way that the formation of reentries is favored. However, a reentry can only be generated by simultaneous decoupling of the cells.

References

[1] Nygren A, Fiset C, Firek L, et al. Mathematical model of an adult human atrial cell: the role of K+ currents in repolarization. Circ Res. 1998; 82: 63-81.

[2] Vanderbrink BA, Sellitto C, Saba S, et al. Connexin40-deficient mice exhibit atrioventricular nodal and infra-Hisian conduction abnormalities. J Cardiovasc Electrophysiol. 2000; 11: 1270-1276.

[3] Tamaddon HS, Vaidya D, Simon AM, et al. High-resolution optical mapping of the right bundle branch in connexin40 knockout mice reveals slow conduction in the specialized conduction system. Circ Res. 2000; 87: 929-936.

[4] Hodgkin AL, Huxley AF. A quantitative description of membrane current and its application to conduction and excitation in nerve (reprint from 1952). Bull Math Biol. 1990; 52: 25-71.

[5] Kenner J, Sneyd J. Mathematical Physiology. Heidelberg: Springer. 1998; 116-135.

[6] Hansson A, Holm M, Blomstrom P, et al. Right atrial free wall conduction velocity and degree of anisotropy in patients with stable sinus rhythm studied during open heart surgery. Eur Heart J. 1998; 19: 293-300.

[7] Hurst JW. The Heart. New York: Mc Graw-Hill Book Company. 1986.

[8] Sugihara K, Iri M. A robust topology-oriented incremental algorithm for voronoi diagrams. Int J Comp Geom & Appl. 1994; 4: 179-228.

[9] Tucker GE, Lancaster ST, Gasparini NM, et al. An object-oriented framework for distributedhydrologic and geomorphic modeling using trinagulated irregular networks. Comput Geosci. 2000; 1-15.

[10] Shaw RM, Rudy Y. Electrophysiologic effects of acute myocardial ischemia. A mechanistic investigation of action potential conduction and conduction failure. Circ Res. 1997; 80: 124-138.

[11] Rudy Y. The ionic mechanisms of conduction in cardiac tissue. J Electrocardiol. 2001; 34(Suppl): 65-68.

[12] Nygren A, Giles WR. Mathematical simulation of slowing of cardiac conduction velocity by elevated extracellular. Ann Biomed Eng. 2000; 28: 951-957.

[13] Sperelakis N. Cell Physiology source book. San Diego: Academic Press. 1998.

[14] Rosen MR. The links between basic and clinical cardiac electrophysiology. Circulation. 1988; 77: 251-263.

[15] Roskamm H, Reindell H. Herzkrankheiten. Berlin: Springer, 1996.

Contact
Dr. Hannes Krätschmer
Department of Biomedical Engineering
Friedrich-Alexander-University
Erlangen-Nuremberg
Turnstrasse 5
D-91054 Erlangen
Germany
Fax: +49 9131 27196
E-mail: hannes.kraetschmer@biomed.uni-erlangen.de